On Growth Rate of Wind Waves: Impact of Short-Scale Breaking Modulations

VLADIMIR KUDRYAVTSEV

Russian State Hydrometeorological University, St. Petersburg, and Marine Hydrophysical Institute, Sebastopol, Russia

BERTRAND CHAPRON

Laboratoire d'Oceanographie Spatiale, Ifremer, Plouzane, France, and Russian State Hydrometeorological University, St. Petersburg, Russia

(Manuscript received 22 October 2014, in final form 17 November 2015)

ABSTRACT

The wave generation model based on the rapid distortion concept significantly underestimates empirical values of the wave growth rate. As suggested before, inclusion of the aerodynamic roughness modulations effect on the amplitude of the slope-correlated surface pressure could potentially reconcile this model approach with observations. This study explores the role of short-scale breaking modulations to amplify the growth rate of modulating longer waves. As developed, airflow separations from modulated breaking waves result in strong modulations of the turbulent stress in the inner region of the modulating waves. In turn, this leads to amplifying the slope-correlated surface pressure anomalies. As evaluated, such a mechanism can be very efficient for enhancing the wind-wave growth rate by a factor of 2–3.

1. Introduction

The wind growth rate of surface waves β is a key to model exchange processes. In particular, the momentum flux to the surface (form drag) τ generally follows

$$\tau = \int \beta V^2 B d\varphi d\ln k,$$

where B is the saturation wave spectrum; k and φ are its wavenumber and its direction, respectively; V is the typical velocity, related to the phase velocity c, for regular nonbreaking waves and related to $u_b = c$ for breaking waves, where u_b is the wind velocity at the height of the breaking crest (see, e.g., Kudryavtsev et al. 2014, hereinafter KCM2014, and references therein).

Wave growth models have been extensively reviewed and compared to experimental results (e.g., Belcher and Hunt 1993; Belcher and Hunt 1998; Janssen 2004; Peirson and Garcia 2008). In brief, Miles (1957) first considered a quasi-laminar approximation to explain the wind-wave growth. Using a mixing length closure (e.g., Gent and Taylor 1976), the impact of turbulence was included but also further criticized, as turbulent eddies in the outer layer are too inertial to transfer momentum on the wave scales. The rapid distortion concept is free of such physical drawbacks, considering the local equilibrium of the turbulence with the wave-induced wind shear to hold in a thin layer [the inner region (IR)] adjacent to the surface (Belcher and Hunt 1993). Following the rapid distortion theory, Miles's critical layer mechanism is then only relevant for fast-moving waves with phase velocity near the wind speed at $z = 10$ m. However, the growth rate predicted by the rapid distortion theory strongly underestimates practical values (e.g., Plant 1982) or those obtained in recent laboratory measurements (Grare et al. 2013). Similar differences were also reported using direct numerical simulations (Sullivan et al. 2000), simulations of the wave growth rate using nonlinear numerical model with second-order closure (Mastenbroek 1996), and large-eddy simulations (e.g., Yang et al. 2013).

The modulation of aerodynamic roughness along the wave profile was suggested as the most plausible candidate to conform the model growth rate to the observations. The impact of varying roughness on the wind-wave growth rate was numerically demonstrated by Gent and

Corresponding author address: Vladimir Kudryavtsev, Russian State Hydrometeorological University, 98 Malookhtinskii, St. Petersburg 195196, Russia.
E-mail: kudr@rshu.ru

DOI: 10.1175/JPO-D-14-0216.1

Taylor (1976) and Maat and Makin (1992). Belcher and Hunt (1993) further investigated the impact of the varying surface roughness prescribed by the Charnock relation and found a weak effect. Mastenbroek (1996) developed a comprehensive model to describe how aerodynamic roughness related to wave-induced stress supported by short waves varies along a long wave and found that the growth of the long modulating wave can be increased by 50%, not enough to conform the model with observations. The airflow separation from short-scale breaking waves was then suggested (Belcher and Hunt 1998), and numerically confirmed (Kudryavtsev and Makin 2002), as the most plausible mechanism. The reason is that breaking of short waves can be strongly modulated by longer waves, up to 20 times (Dulov et al. 2002). As the airflow separation from the breaking crests of short waves supports a significant part of the form drag (Makin and Kudryavtsev 2002; KCM2014), strong wave breaking modulations and related modulations in the aerodynamic roughness may then significantly enhance the growth rate of the modulating wave (by factor of about 2; Kudryavtsev and Makin 2002). Another possibility for enhancing the growth rate is to consider the effect of wave grouping, discussed by Hunt et al. (2011).

In this paper, the KCM2014 coupled model is thus used to highlight how significant the impact of small-scale breaking modulation, and the resulting modulated stress, can be on the growth rate of larger modulating waves.

2. Basic relations

The energy transfer from wind to waves results from the work of surface pressure p_s against wave vertical velocity u_{s3}, work of the surface stress $\tau_{s\alpha}$ against horizontal velocity $u_{s\alpha}$, and work of the radiation wave stress $S_{s\beta}$ against gradients of the horizontal wave orbital velocity $\partial u_{s\alpha}/\partial x_\beta$ (e.g., Garrett and Smith 1976; Kudryavtsev and Makin 2002):

$$\partial E_w/\partial t = \rho_a\langle p_s u_{s3}\rangle + \rho_a\langle \tau_{s\alpha}u_{s\alpha}\rangle + \langle S_{\alpha\beta}\partial u_{s\alpha}/\partial x_\beta\rangle, \qquad (1)$$

where E_w is the wave energy. Hereinafter, surface pressure p_s and stress $\tau_{s\alpha}$ are scaled by air density ρ_a, subscripts α and β refer to horizontal components, and the angle braces denote an average over the wave scales. Stress $\tau_{s\alpha}$ in (1) includes both momentum flux to modulated shorter waves and shear viscous stress acting on the surface. The energy gain provided by $\langle\tau_{s\alpha}u_{s\alpha}\rangle$ is equivalent to Longuet-Higgins's (1969) maser mechanism (see Garrett and Smith 1976 for more discussion). As already reported (e.g., Garrett and Smith 1976; Kudryavtsev and Makin 2002), the impact of the wave radiation stress is weak and is therefore ignored. For simplicity, we consider one-dimensional situation; that is, wind and waves are aligned. The dimensionless growth rate, $\beta = (wE)^{-1}\partial E/\partial t$, then reads

$$\beta = (\rho_a/\rho_w)c^{-2}(\hat{p}_s^I + \hat{\tau}_s^R), \qquad (2)$$

where ρ_w is the water density; hereinafter, the hat over any quantity denotes its Fourier amplitude scaled by ak (where a is the amplitude of the wave surface), and superscripts "R" and "I" indicate the real and imaginary parts, respectively.

To calculate β using (2), the amplitudes of the surface pressure and stress can be defined as the output of an atmospheric turbulent boundary layer model over the wave, which (for the sake of completeness) should be coupled with short waves modulated by this longer wave [see, e.g., numerical model simulations by Mastenbroek (1996) and Kudryavtsev and Makin (2002)]. The present development employs an analytical model approach based on the aggregation of two models: (i) the model of the turbulent shear flow over slowly moving waves by Belcher and Hunt (1993) and (ii) the coupled wind-wave model suggested by KCM2014.

Except for the fast-moving waves, with phase velocity comparable to the 10-m wind speed u_{10}, the amplitude of the slope-correlated component of the surface pressure $\hat{p}_s^I$ originates from dynamics of the turbulent stresses inside the IR adjacent to the surface and is proportional to the elevation-correlated component of the surface stress $\hat{\tau}_s^R$ (Belcher and Hunt 1993, p. 131):

$$\hat{p}_s^I \propto (U_m/U_l)^2\hat{\tau}_s^R, \qquad (3)$$

where $U_m = \overline{u}_m - c$, $U_l = \overline{u}_l - c$, $\overline{u}_m$, and $\overline{u}_l$ are mean wind velocity at a middle-layer height, $z = h_m$, and at the IR height, $z = l$. Heights of the IR, l, and the midlayer, h_m, are defined as $kl = 2\kappa u_*/U_l$, and $kh_m = [u_*/(\kappa U_m)]^{1/2}$, where u_* is the air friction velocity and κ is the Kármán constant.

Modulation of the surface stress is then decomposed as

$$\hat{\tau}_s^R = \hat{\tau}_U^R + \hat{\tau}_S^R, \qquad (4)$$

where $\hat{\tau}_U^R$ are undulations of the airflow over the wave profile,

$$\hat{\tau}_U^R/u_*^2 = 2U_m^2/U_l^2, \qquad (5)$$

and $\hat{\tau}_S^R$ results from the adherence of the airflow to the surface velocity ($\hat{u}_s$):

$$\hat{\tau}_S^R/u_*^2 = -2\hat{u}_s/U_l. \qquad (6)$$

Both effects generate slope-correlated surface pressure [(3)], defined as

$$\hat{p}^I = (U_m^2/U_l^2)(2\hat{\tau}_U^R + \hat{\tau}_S^R). \tag{7}$$

The resulting dimensionless growth rate [(2) with (4) and (7)] then reads [Belcher and Hunt 1993, their (5.19) in zero order on u_*/U_l]

$$\beta = 2\frac{\rho_a}{\rho_w}\frac{U_m^2}{U_l^2}\left[\left(2\frac{U_m^2}{U_l^2}+1\right) - \frac{\hat{u}_s}{U_l}\left(1+\frac{U_l^2}{U_m^2}\right)\right]\frac{u_*^2}{c^2}. \tag{8}$$

Thus, the growth rate of wind waves, due to the work of either normal or tangential stresses, results from the modulation of the turbulent stress inside the IR caused by the airflow undulations over the wavy surface (the first term in the square bracket) and the surface horizontal velocity oscillations (the second term in the square bracket).

Aerodynamic roughness modulations can be readily taken into account via the surface velocity variations, $\hat{u}_s$. Under linear approximation, variations of the surface roughness scale, $z_0 = \overline{z}_0 + \widetilde{z}_0$ (where $\overline{z}_0$ is the mean value and $\widetilde{z}_0$ is modulation), lead to [Belcher and Hunt 1993, their (4.1)] $\hat{u}_s = c - (u_*/\kappa)\hat{z}_0/\overline{z}_0$. In terms of modulations of the drag coefficient, c_{dl}, for the IR, the roughness scale modulations are expressed as $\hat{z}_0/\overline{z}_0 = 1/2(\kappa U_l/u_*)\hat{c}_{dl}/\overline{c}_{dl}$. Then the surface velocity becomes

$$\hat{u}_s = c - 1/2U_l(\hat{c}_{dl}/\overline{c}_{dl}) \tag{9}$$

and the growth rate [(8)] now reads

$$\beta = C_\beta\frac{\rho_a}{\rho_w}\frac{u_*^2}{c^2},$$
$$C_\beta = 2\frac{U_m^2}{U_l^2}\left[\left(2\frac{U_m^2}{U_l^2}+1\right) - \left(\frac{c}{U_l} - \frac{\hat{c}_{dl}}{2\overline{c}_{dl}}\right)\left(1+\frac{U_l^2}{U_m^2}\right)\right], \tag{10}$$

where C_β is a growth rate parameter. From (10), variations of z_0 (or the drag coefficient) in phase with surface elevations will amplify the growth rate.

First reported by Gent and Taylor (1976), using a rather different numerical model, a threefold β amplification was found for z_0 varying along the wave within ±75% of its mean value. Smith (1986), analyzing modulations of radar backscatter by surface waves, concluded that the observed strong short-wave modulation is associated with wind stress variations. The implied modulations of wind stress were rather large, on the order of 10 times the wave steepness. Smith (1986) also emphasized how implied strong modulations could enhance the wave growth rate. Yet, no mechanism leading to strong stress modulations was suggested. Belcher and Hunt (1993) used the Charnock relation, $z_0 \propto u_*^2/g$, to evaluate the impact of z_0 modulations. Modulations of the roughness scale are linked to the stress modulations as follows: $\hat{z}_0/\overline{z}_0 = \hat{\tau}/u_*^2$, which is equivalent to $\hat{c}_{dl}/(2c_{dl}) = (\hat{\tau}/u_*^2)/\ln(l/z_{cr})$. Since $\hat{\tau}/u_*^2 \approx 2U_m^2/U_l^2$, the contribution of these modulations to β is small [on the order of $\ln^{-1}(l/z_{cr})$] compared to the contribution of the airflow undulations described by the first term in the square bracket in (10).

As a reference model calculation, Fig. 1a shows the model growth rate [(10)] for constant z_0 prescribed by the Charnock relation: $z_0 = 0.015 \times u_*^2/g$. The main contribution comes from the work of the surface pressure, while the contribution of the surface stress work against the wave orbital velocity is less efficient. As already reported (e.g., Belcher and Hunt 1998, their Fig. 8), the resulting growth rate significantly underestimates empirical values (e.g., Plant 1982). Recent laboratory measurements (Peirson and Garcia 2008; Grare et al. 2013) provide further evidence of higher values, especially at small wave steepness, from about $C_\beta = 50$ to $C_\beta = 80$, with a clear decreasing trend with increasing wave steepness (C_β drops to $C_\beta \approx 20$ at rather large $ak \approx 0.3$).

As developed, the model [(10)] applies to waves whose critical height, z_{cr} [the height where the phase velocity is equal to the wind speed, $\overline{u}(z_{cr}) = c$], lies well inside the IR. Such a condition is valid for rather "slow" waves with smaller phase velocities, by a factor of 1.5–2 (and more), and with a wind speed at 10-m height, u_{10}. For faster waves, dynamics of the critical height should dominate the wave growth rate (Miles 1957). In this case, β reads as

$$\beta = \frac{\pi k z_{cr}}{2\kappa^2}\left[\int_{kz_{cr}}^{\infty}(\kappa U/u_*)^2 e^{-kz}d(kz)\right]^2. \tag{11}$$

In the overlapping range of inverse wave ages (around $u_{10}/c = 2$), the growth rate [(11)] is consistent with empirical values and significantly exceeds β predicted by the nonseparated sheltering mechanism [(10); see Fig. 1a]. While contradicting the original assumptions, Miles's growth rate is thus often extended to the spectral range of slow waves to match empirical relationships for practical applications (Janssen 2004).

3. Impact of surface roughness modulations

In KCM2014, the impacts of both regular (nonbreaking) and breaking waves on the sea surface drag are considered. The spectral contribution of the nonbreaking waves (via wave-induced momentum flux) and breaking

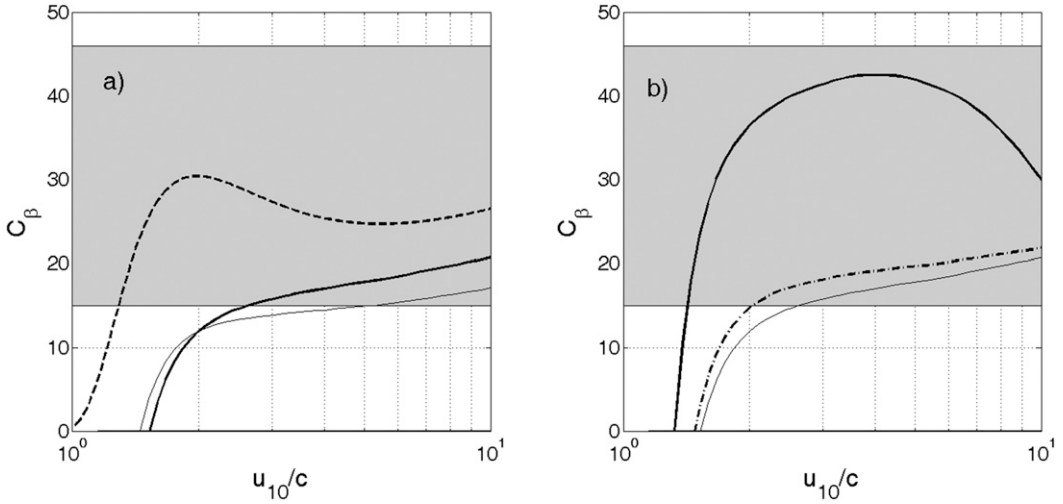

FIG. 1. The wind-wave growth rate parameter, $C_\beta = (\rho_w/\rho_a)(c^2/u_*^2)\beta$, vs inverse wave age, u_{10}/c, at wind speed $u_{10} = 10\,\mathrm{m\,s^{-1}}$. (a) Growth rate parameter following the sheltering mechanism [(10)] with constant z_0 (thick solid line) and Miles's mechanism [(11); dashed line]. Growth rate C_β [(10)] due to work of the surface pressure only (thin solid line). (b) Growth rate following the sheltering mechanism [(10)]: constant z_0 (thin solid line) and the varying surface roughness but without accounting for the wave breaking modulations (dashed–dotted line) and with varying surface roughness accounting for the wave breaking modulations, (10) with (15) (thick solid line). Shaded area indicates the range of expected empirical values (Plant 1982).

waves (via the airflow separations), and their integral impact on the form drag of the sea surface are illustrated in Figs. 3 and 4 in KCM2014. A dimensionless form drag function F is introduced to describe the sheltering of the turbulent airflow by the waves, leading to changes of the vertical distribution for the turbulent stress $\tau(z)$:

$$\tau(z)/u_*^2 = \exp\left(-\int_z^\infty F d\ln z\right). \tag{12}$$

The form drag function is further decomposed between the impact of nonbreaking and breaking waves to the sheltering of the turbulent airflow, as

$$F(z) = [c_w B_0(k)]_{k=\varepsilon_l/z} + [c_s(\overline{u}_b/c - 1)^2 B_0(k)]_{k=\varepsilon_b/z}, \tag{13}$$

where B_0 is the omnidirectional saturation spectrum, $\varepsilon_l = kl$ is the dimensionless height of the IR (on the order of 0.1), ε_b is the dimensionless height of the breaking wave crest, $\overline{u}_b$ is the mean wind speed at the height of a breaking crest, and c_w and c_s are model constants (see KCM2014 for more details). The first term in (13) corresponds to the nonbreaking contribution, and the second term takes into account the breaking waves.

Accordingly, the surface drag coefficient C_{Dh} defining the friction velocity u_* in the core of the boundary layer $u_*^2 = C_{Dh}\overline{u}_h^2$ as a function of the wind speed $\overline{u}_h = \overline{u}(h)$ at reference level $z = h$ becomes

$$C_{Dh} = \left[\kappa \Big/ \int_0^h \exp\left(-3/4\int_z^\infty F d\ln z\right)(1 + z_{0\nu}/z)^{-1} d\ln z\right]^2, \tag{14}$$

where $z_{0\nu}$ is the viscous roughness scale. If $F = 0$, then the classical drag coefficient for a smooth surface is recovered. Figure 1 in KCM2014 illustrates model calculations of the drag coefficient and a comparison with the observations.

We can then consider a long wave (LW) with wavenumber K modulating shorter waves (SWs) in the spectral range $k > k_m = mK$, where m is a large number. This scale division between modulating LWs and modulated SWs must ensure that both the wave-induced and the airflow separation stress supported by these SWs are well confined within the LW IR of height $L = \varepsilon_l/K$. Following KCM2014, the airflow separation affects a layer $z < \varepsilon_b/k$ with $\varepsilon_b = 0.3$. Accordingly, the wavenumber range of modulated SWs, k_m, must be $k_m > (\varepsilon_b/\varepsilon_l)K \approx 3K$. Modulation of the momentum flux to these SWs leads to modulations of the LW IR drag coefficient, $\hat{c}_{dL}/c_{dL}$, which can be found from (14). Expanding (14) into a series of small variations of F and using (12), the first-order correction of the drag coefficient in the LW IR is

$$\frac{\hat{c}_{dL}}{c_{dL}} = \frac{3}{2}\frac{\displaystyle\int_0^L (1 + z_{0\nu}/z)^{-1}\tau^{3/4}\int_z^L \hat{F}\, d\varsigma'\, d\varsigma}{\displaystyle\int_0^L (1 + z_{0\nu}/z)^{-1}\tau^{3/4}\, d\varsigma}, \tag{15}$$

where variable ς is $\varsigma = \ln z$, τ is a local turbulent stress defined by (12), and $\hat{F}$ is the Fourier amplitude of modulations of the SW form drag function:

$$\hat{F}(z) = (c_w B_0 M^R)_{k=\varepsilon_l/z} + [c_s(\overline{u}_b/c-1)^2(n+1)M^R B_0]_{k=\varepsilon_b/z}, \tag{16}$$

where $M = \hat{B}_o/B_o$ is the SW spectral modulation transfer function (MTF), with superscript R to indicate the real part. To derive this expression, we took into account that the length of wave breaking fronts, $\Lambda(k)$, is a nonlinear function of the saturation spectrum: $\Lambda \propto k^{-1}B^{n+1}$, where n is a dissipation parameter (Phillips 1985). The modulations of the form drag of SWs breaking are thus amplified by a factor $(n + 1)$ relative to the spectrum MTF: $\hat{\Lambda}/\Lambda = (n + 1)M$. LW-induced variations of the wind speed are ignored. The MTF associated with these variations, $M_{u_b} = \hat{u}_b/\overline{u}_b$, is indeed on the order of $M_{u_b} \approx 1$, which is much weaker (a factor of order 10) than the effect of wave breaking modulations.

The spectral MTF accounting for both the interaction of SW with orbital velocities of LW and the effect of SW wind forcing modulations leads to [see, e.g., (24) in Kudryavtsev and Makin 2002]

$$M = -\left(\frac{1-ir}{1+r^2}\right)\frac{k_1}{N}\frac{\partial N}{\partial k_1} + \frac{r+i}{1+r^2} r_* M_\beta, \tag{17}$$

where N is the wind-coupled wave action spectrum, $N = \omega k^{-5}B$, and $r = nr_*$ is the relaxation parameter; $r_* = \beta\omega/\Omega$ is the SW growth rate scaled by LW frequency Ω, ω is the SW frequency, and $M_\beta \equiv \hat{\beta}/\overline{\beta}$ is the SW wind forcing MTFs. Following KCM2014, the growth rate of SWs is $\beta \propto \tau(z)/c^2$, where $\tau(z)$ is the local turbulent shear stress at $z = \varepsilon_l/k$ defined by (12), which accounts for the sheltering by longer waves. The SWs wind forcing MTF M_β becomes

$$M_\beta = M_\tau - \int_z^L \hat{F} d\ln z \Big/ \exp\left(-\int_z^L F d\ln z\right)$$
$$M_\tau \equiv \widehat{u_*^2}/\overline{u_*^2} = 2(U_m^2/U_l^2 - c/U_l) + \hat{c}_{dl}/\overline{c}_{dl}, \tag{18}$$

where M_τ is the total stress MTF in the LW IR. Modulations of the SW growth rate are thus caused by two opposing mechanisms: total stress modulations, due to the airflow undulations and modulation of the aerodynamic roughness, lead to enhancement of the wind forcing; however, enhancement of wave breaking increases the sheltering of shorter waves to finally prevent wind forcing enhancement. Posterior calculations confirm that these factors almost compensate for each other, with a very weak combined impact on the SW modulations as compared to the interactions of SWs with LW orbital velocities. We thus ignore the second term in (17). This is, in some way, at variance with previous model analysis (Smith 1986; Mastenbroek 1996; Kudryavtsev and Makin 2002), for which the surface stress MTF, M_τ, was the main source of SW modulation. In the present model, the large anticipated M_τ on the SW modulations via wind forcing is inhibited by the sheltering of SWs from modulated breaking waves.

To note, the spectral angular distributions of the form drag model is narrow: the wave-induced stress is proportional to $\cos^3\varphi$ and the airflow separation stress is proportional to $\cos^5\varphi$, where φ is the direction of the wavenumber vector relative to the wind direction [see (9) and (18) in KCM2014]. Moreover, the term $\partial \ln N/\partial \ln k_1$ in the MTF [(17)] is $\partial \ln N/\partial \ln k_1 \propto \cos^2\varphi$. Thus, the spectral components traveling in the wind direction provide the main contribution to the form drag modulations. Following this reasoning and for the sake of simplicity, we take (17) in the wind direction to evaluate the aerodynamic roughness modulations:

$$M^R = -m_k(1+r^2)^{-1}, \tag{19}$$

where $m_k = \partial \ln N(\varphi_w,k)/\partial \ln k$ is the wavenumber exponent of the wave action spectrum in the wind direction and superscript R stands for the real part. Away from the spectral peak, the exponent m_k can be evaluated as $m_k \approx -9/2$. MTF [(19)] is valid in the SW spectral range $k > k_m = mK$, taking $M^R = 0$ outside this range (in further calculations we define m as $m = 5$). Thus, elevation-correlated modulation of the SW spectrum [(19)] leads to variation of the surface drag coefficient (aerodynamic roughness) along the modulating LW, (15) with (16), that in turn amplifies the growth rate of LW as it is predicted by (10).

It is worthwhile to emphasize the following. SW modulation provides a dual impact on LW growth. The first impact results from the work of SW stress against orbital velocity, the second term in (1). This is the so-called maser mechanism of wave generation (Longuet-Higgins 1969). The second impact originates from the relation of the slope-correlated pressure to the elevation-correlated shear stress [(7)], which includes SW stress. Therefore, SW modulations also impact the wave growth via the work of the surface pressure described by the first term in (1). These effects are all included in (10), as the term $(\hat{c}_{dl}/2c_{dl})(1 + U_l^2/U_m^2)$ sums up the SW stress impact via the work of the surface pressure and the maser mechanism, correspondingly. Since U_l^2/U_m^2 is about 0.4, the impact on the growth rate via the amplification of the slope-correlated pressure is more efficient (by a factor of about 2.5) than the impact via the maser mechanism.

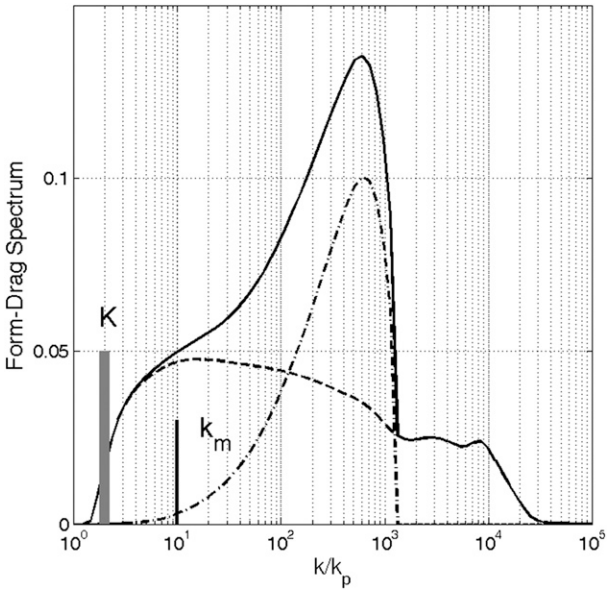

FIG. 2. Spectra of the form drag (solid line), its component supported by wave-induced momentum flux to regular waves (dashed line), and airflow separations from breaking crests (dashed–dotted line). Vertical thick gray and black lines show an example of the modulating LW with wavenumber $K = 2k_p$ (k_p is the spectral peak wavenumber) and the range of modulated SWs, $k > k_m = 5K$.

4. Some results

a. Developed seas

We wish to evaluate the impact of SW modulations on the growth rate of the energy-containing waves for developed wind seas, when $u_{10}/c_p \approx 1$, c_p is the phase velocity of the spectral peak. The spectral distribution of the form drag supported by the wave-induced momentum flux to the nonbreaking waves and the airflow separation from crests of breaking waves at $u_{10} = 10\,\mathrm{m\,s^{-1}}$ is shown in Fig. 2. In this case, the form drag constitutes 57% of the total drag, 35% is provided by nonbreaking waves, and 22% is provided by breaking waves; see Fig. 3 in KCM2014. As it follows from Fig. 2, the main contribution to the form drag due to the airflow separations is coming from the shortest breaking waves. Hence, a large spectral gap separates energy-containing waves from shorter waves, providing a major contribution to the form drag. With increasing LW wavelength, the wavenumber range of modulated SW further shifts toward the shorter scale. For example, if $K/k_p = 20$, then the range of modulated SWs, $k/k_p > k_m/k_p = 10^2$, still supports half of the total form drag and a major portion of the airflow separation stress. The portion of the form drag supported by modulated SWs gradually decreases with increasing K/k_p. For K/k_p exceeding $K/k_p = 2 \times 10^2$, modulated SWs do not contribute to the airflow separation stress. In this case, modulations of the aerodynamic roughness along LWs should almost vanish.

Figure 1b shows the effect of SW modulations on the LW growth when the effect of wave breaking on the aerodynamic roughness modulations is switched off [the second term on the rhs of (16) is omitted]. Without airflow separations, the wave-induced stress modulations alone provide weak impacts on drag coefficient modulations, and thus on the LW growth rate. Similar result were found by Mastenbroek (1996) within the frame of a comprehensive numerical atmospheric boundary layer model over LWs coupled with SWs, via the surface drag provided by SW-induced momentum flux. In addition to the straining mechanism [the first term in (17)], Mastenbroek (1996) also included the SW growth rate modulations [the second term in (17)] associated with the surface stress modulations. The latter mechanism (via feedback between SWs and surface stress) significantly enhanced the SW modulations. However, such enhanced SW modulations and associated aerodynamic roughness modulations only lead to increasing the LW growth rate by 50%, still smaller than estimates from observations. In the present simulations, we do not include the impact of SW growth rate modulations on the MTF. As already argued above [see (18)], modulations of the surface stress and the effect of the SW sheltering compensate for each other, leading to weak modulation of the SW growth rate. Our simulations based on a "truncated" SW MTF [(19)] lead to an increase in the LW growth rate by 25% (in the range of u_{10}/C from 2 to 3; see Fig. 1b)—of the same order as obtained by Mastenbroek (1996).

Let us now turn to the SW breaking modulations and associated modulations in the airflow separation stress. As it follows from (16), the magnitude of the modulation of the airflow separation stress is dependent on the wave breaking parameter n. The same parameter also defines the shape of the equilibrium gravity wave spectrum, $B \propto (u_*/c)^{2/n}$, and n can be derived from spectral measurements, ranging from $n = 2$ (Phillips 1985; Elfouhaily et al. 1997) to $n = 5$ (Donelan and Pierson 1987) and $n = 10$ (Banner at al. 1989; Yurovskaya et al. 2013). Figure 3 illustrates the effect of this wave breaking parameter n on the modulation of the IR drag coefficient [(15)] and the growth rate of LW [(10)]. Modulation of SW breaking drastically enhances (as compared with c_{dL} variations caused by nonbreaking SWs) variations of the aerodynamic roughness (drag coefficient) along the modulating LW at any n value. The LW growth rates for different values of n are shown in Fig. 3b. A strong impact of wave breaking exists for all plausible values of n. The LW growth increases with increasing n but with a significantly lower amplification than $(n + 1)$, as

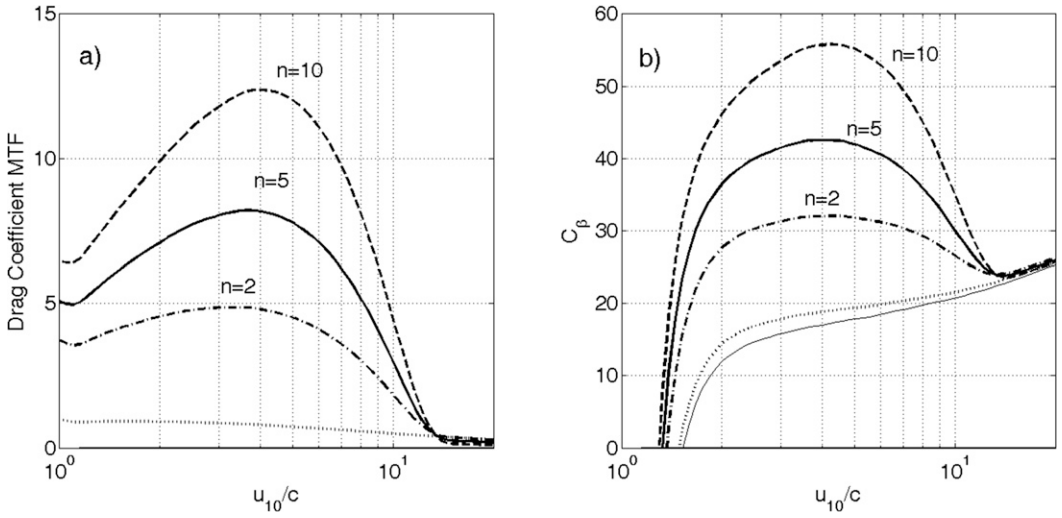

FIG. 3. (a) Dependence of the real part of the drag coefficient MTF [(15)], $M_d = \hat{c}_{dL}/c_{dL}$, on wave breaking parameter n (indicated in the plot) and $M_d = \hat{c}_{dL}/c_{dL}$ if the modulation of wave breaking is ignored [second term in (16) is omitted; dashed–dotted line]. (b) Dependence of the LW growth rate on wave breaking parameter n: C_β if the impact of wave breaking on modulations of aerodynamic roughness z_0 is ignored (dotted line) and C_β at constant z_0 (thin solid line).

expected from (10) with (16). This comes from the dependency of the relaxation parameter r on n in MTF [(19)]. Asymptotically, at $n \to \infty$, the impact of wave breaking on LW growth rate vanishes due to an overall shift of wave breaking modulations on the forward slope of the modulating LW.

Field measurements of SW whitecap modulations by longer surface waves by Dulov et al. (2002) revealed strong modulations of whitecap coverage by LW, with an MTF of about 20 (their Fig. 2). This estimate can be used to assess a plausible value of the wave breaking parameter n. The model whitecap MTF, M_q, is defined as

$$M_q = (n+1)\int_{k<k_{wc}} M\,dq \Big/ \int_{k<k_{wc}} dq, \qquad (20)$$

where $dq \propto k^{-2}\beta B dk$ is the fractional whitecap coverage from breaking waves in wavenumber interval dk (Phillips 1985) and k_{wc} is the wavenumber of the shortest breaking waves generating measurable whitecaps (fixed here as $k_{wc} = 2\pi/1\,\mathrm{rad\,m^{-1}}$; wavelength is 1 m). Using (20), the data shown in Fig. 4 suggest that $n = 5$ is a reasonable value. Model simulations of the growth rate in (10) with (15) and (16) for $n = 5$ are shown in Fig. 1b. Accounting for the aerodynamic roughness variations caused by SW breaking modulations significantly enhances the growth rate and reconciles the nonseparate sheltering mechanism of wave generation with observations.

Figure 5 further illustrates the wind speed dependence of the growth rate. The reference growth rate (with z_0 constant) is almost wind speed independent. As the contribution of the airflow separations to the total stress is strongly wind dependent (it increases from 5% to 45% in wind speed range from 5 to 20 m s^{-1}; see, e.g., Fig. 3 in KCM2014), the impact of wave breaking modulations

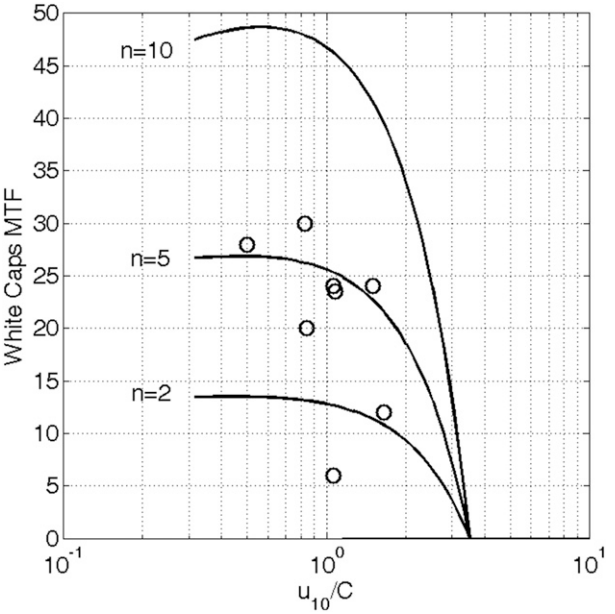

FIG. 4. MTF of the whitecaps of short-scale breaking waves vs inverse wave age of modulating wave. Field measurements (open circles) by Dulov et al. (2002). Model calculations using (20) for different values of wave breaking parameter n at 10 m s^{-1} wind speed (lines).

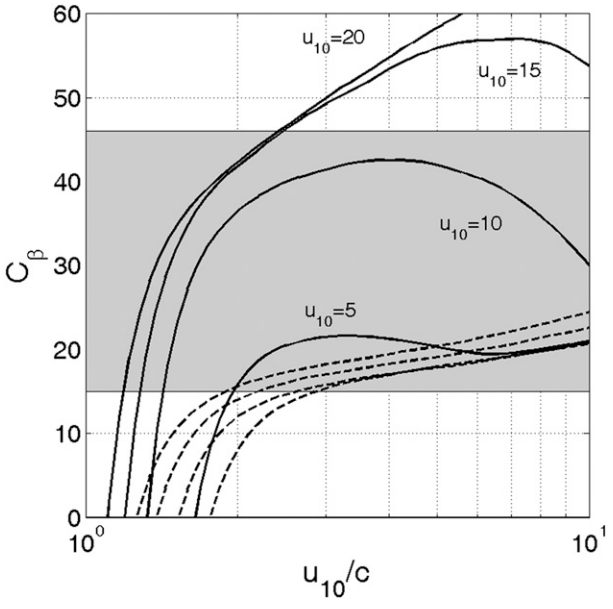

FIG. 5. LW growth rate parameter C_β at different wind speeds: 5, 10, 15, and 20 m s^{-1}. Full model for indicated wind speed (solid line); C_β at constant z_0 (dashed line; C_β increases with increasing wind speed). Range of expected empirical values (shaded; Plant 1982).

on LW growth rate rapidly increases with increasing wind. However, a saturation of the LW growth rate at the highest model wind speeds (15 and 20 m s^{-1}) is noticeable. This also relates to the continuous shift of wave breaking modulations from the crests of modulating waves to their forward slope with increasing wind speed. Notice also that at high wind speeds, crests of short breaking waves can probably be aerodynamically disrupted (pulverized to droplets), which in turn could lead to diminution of the impact of SW form drag modulations on the LW growth rate. Therefore, we may speculate that growth rate curves for high winds in Fig. 5 overestimate "real" values.

All growth rate estimates, Figs. 1 and 5, are derived using small perturbations in the coupled wind-wave system caused by long-wave components from "typical" developed sea spectra. Modifications of the wave field spectrum (i.e., introduction of swell or a mechanically generated wave, or enhancement/suppression of the long-wave steepness due to other physical mechanism) shall then alter the typical coupled wind-wave system and the spectral redistribution of the form drag components (e.g., due to changes in the sheltering of short-scale waves by longer ones). This will affect the growth rate; that is, it will lead to an explicit dependence on the long-wave steepness. Below, we consider how the wind-induced growth rate of mechanically generated wave depends on its steepness.

b. Laboratory conditions

Peirson and Garcia (2008) and Grare et al. (2013) investigated, in laboratory conditions, the wind-induced growth of mechanically generated waves (LWs), which are slow relative to the wind ($C < u_{10}$ where C is the LW phase velocity). A systematic decrease of the LW growth rate with its steepness increase, KA, was found in both studies (see Fig. 8). At large KA, the LW growth rate matches the model predictions for the constant aerodynamic roughness; however, at small KA, growth rate β is amplified by a factor of 3 or 4. For both experiments, it is apparent that mechanically generated waves significantly damp the wind-wave energy (see, e.g., Fig. 2 in Peirson and Garcia 2008). Following this observation, we may relate the dependence of the LW growth on its steepness with the suppression of wind-generated waves and the associated variations of the aerodynamic roughness along the modulating LW.

For the same laboratory conditions as reported in Grare et al. (2013), Makin et al. (2007) analyzed measurements of the turbulent stress above a mixed wave field (wind-generated plus mechanically generated waves). With the introduction of LWs, a decrease in the stress is reported, essentially caused by the suppression of wind-generated waves and their contribution to the form drag. An increase of the LW steepness then augments the stress due to the increasing contribution of the LW-induced stress to the form drag.

The model suggested in section 2, without modification, is used to simulate and to interpret these measurements reported by Peirson and Garcia (2008) and Grare et al. (2013). To adjust the model to the observations, we define the spectral peak f_p of wind-generated waves as

$$2\pi f_p u_{10}/g = 14.8\tilde{x}^{-0.27}, \tag{21}$$

where $\tilde{x} = xg/u_{10}^2$ is the dimensionless fetch. Relation (21) fits the observed peak frequency at fetch 28 m, reported in Grare et al. (2013, see their Table 1, runs U4F0–U49F0). Experimental estimates of the growth rate were derived from the observed energy development of mechanically generated waves with fetch. Short wind-generated waves (SWs) riding on the LWs are also developing with the fetch. Therefore, they have a different wave age in the course of the LW development. For the sake of simplicity, we define a mean (equivalent) short wind-wave field that will be used to further simulate the effect of SWs on LW growth. To that end, we introduce a mean frequency of the wind waves $\overline{f}_p$ by averaging (21) over x, giving $\overline{f}_p = f_p/(1 - 0.27)$.

The saturation spectrum and the spectrum of the form drag for the pure wind-wave conditions are

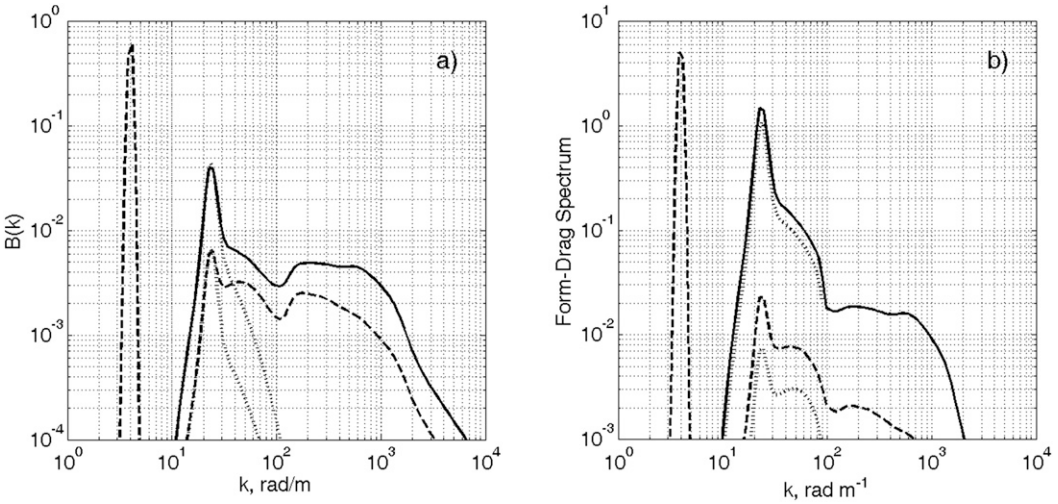

FIG. 6. (a) Model omnidirectional saturation spectra for pure wind waves (solid line), wind-generated waves plus mechanically generated wave (dashed line), and dominant wind-wave spectra (dotted line). (b) Form drag spectra (sum of wave-induced and airflow separation stress scaled by square friction velocity) for pure wind waves (solid line) and wind waves plus mechanically generated wave (dashed line). Dotted lines show the airflow separations components. Conditions: wind speed is $u_{10} = 10\,\mathrm{m\,s^{-1}}$; frequency and steepness of the mechanically generated wave are $F = 1$ Hz and KA = 0.3, respectively; and fetch is 28 m.

shown in Fig. 6. The wind-wave spectrum in KCM2014 is represented as a sum of the energy-containing wave spectrum, B_{lw}, and the equilibrium spectrum, B_{sw}: $B = \chi B_{lw} + (1 - \chi)B_{sw}$, where χ is a cutoff function. The energy-containing component of B is shown in Fig. 6a with dotted line. At this condition ($u_{10} = 10\,\mathrm{m\,s^{-1}}$; KA = 0), the form drag supports 60% of the total stress (Fig. 7b). A major portion of the form drag, 70%, is supported by the airflow separations from breaking crests, and the rest, 30%, is provided by the wave-induced flux to the capillary–gravity waves (Fig. 7b).

Introduction of the mechanically generated wave to the wind waves results in the reduction of wind-wave energy—the effect that had been observed by many investigators [see, e.g., Makin et al. (2007) and Grare et al.

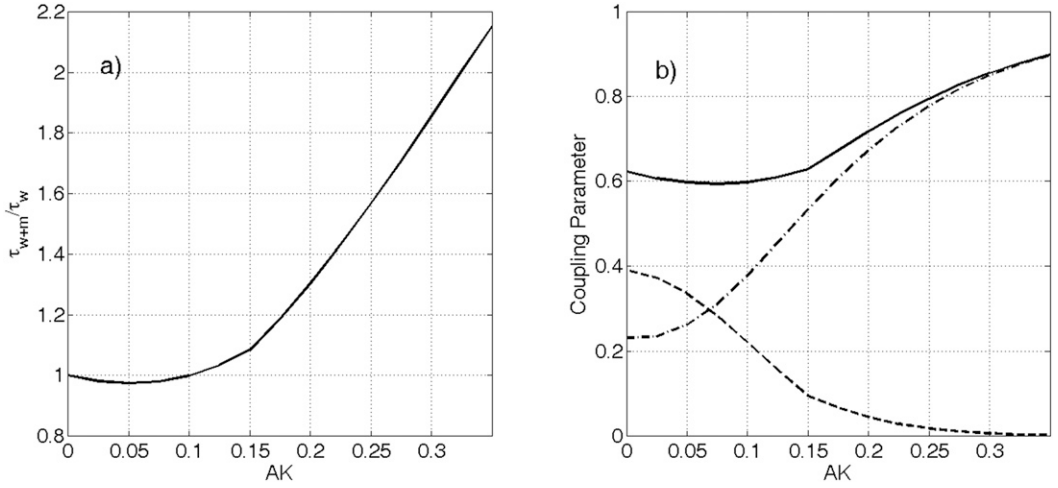

FIG. 7. (a) Ratio of the total stress above wind-generated plus mechanically generated (LW) wave fields, τ_{w+m}, to the stress, τ_w, over pure wind-generated waves vs the LW steepness. (b) Ratio of the form stress and its components, wave-induced (dashed–dotted line) and airflow separation stress (dashed line) to the total stress coupling parameter vs the LW steepness (solid line). Conditions: wind speed is $u_{10} = 10\,\mathrm{m\,s^{-1}}$, LW frequency is $F = 1$ Hz, and fetch is 28 m.

(2013) for references]. Makin et al. (2007, their Fig. 3) quantified this LW impact via a damping factor, and we consider the measured factor as

$$F(\mathrm{AK}) \equiv E_w/E_{w0} = \max(1 - 5.7\mathrm{AK}, 0.15), \quad (22)$$

where E_w is the wind-wave energy in the presence of LW of steepness AK and E_{w0} is the energy of pure wind waves for the same wind speed. Following Makin et al. (2007), we introduce this empirical damping factor in the wind-wave spectrum model as

$$B(k, \mathrm{AK}) = F(\mathrm{AK})\chi B_{lw}(k) + (1 - \chi)B_{sw}(k). \quad (23)$$

This spectral model is further used to investigate the adjustment of the coupled wind-wave system to the introduction of LW and LW growth rate.

An example of the model wind-wave spectrum and the spectrum of the form drag in the presence of LW with KA = 0.3 is shown in Fig. 6a. Notice that the suppression of dominant waves (dotted line) is imposed by the damping factor [(22)], while the drop of the equilibrium spectrum (by a factor of about 2–3) is apparently caused by the sheltering of the short wind-waves by the LW—in line with Chen and Belcher (2000). In the presence of LW, the spectral distribution of the form drag drastically changes (Fig. 6b). Now, most of the form drag is supported by the LW-induced flux. This effect shelters wind waves and results in a weak impact (including wave breaking) to the form drag.

Figure 7 illustrates the main model peculiarities of the stress distribution above the mixed wave field—wind-generated waves plus LW. Introduction of LW of low steepness first leads to some decrease of the stress (relative to the stress over pure wind waves), and then to its growth (at KA > 0.1) due to an increasing contribution of the LW-induced stress to the form drag. This is similar to what was first observed by Peirson et al. (2004) and then simulated by Makin et al. (2007). Calculations (Fig. 7b) suggest that some decrease of the total stress at small KA is caused by the fast suppression of the form drag supported by the airflow separations from breaking crests. At KA > 0.15, the contribution of the airflow separations becomes negligible. Calculations of the coupling parameter in Fig. 7b are consistent with data reported in Grare et al. (2013, their Fig. 5).

Accordingly, the systematic decrease of the growth rate (Fig. 8) and the suppression of the wave breaking (Fig. 7b) can be explicitly linked. As the steepness of the LW is small and the wind-generated waves are not too strongly suppressed, modulations of wave breaking

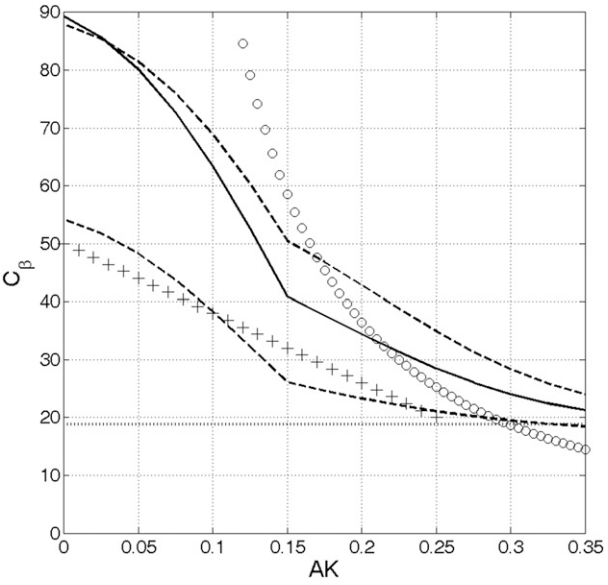

FIG. 8. Growth rate parameter C_β as a function of the wave steepness. Best fits of the growth rate measurements reported by Peirson and Garcia (2008; crosses) and Grare et al. 2013; open circles). Model simulations of the wave growth rates: $u_{10} = 10\,\mathrm{m\,s^{-1}}$ (solid line), $u_{10} = 13\,\mathrm{m\,s^{-1}}$ (upper dashed line), and $u_{10} = 7\,\mathrm{m\,s^{-1}}$ (lower dashed line). Model growth rate for constant aerodynamic roughness (dotted line). Fetch is 28 m, and the frequency of the mechanically generated wave is 1 Hz.

and associated variations of the aerodynamic roughness along the LW surface provide rapid wind-induced growth of the LW. At large KA, wind-generated waves and wave breaking are suppressed, and the associated form drag almost vanishes (see Figs. 6b and 7b). The LW surface almost becomes a smooth surface with constant aerodynamic roughness, with decreasing LW growth. Model simulations for laboratory conditions (Fig. 8) are thus consistent with the measurements. The model reproduces large values of β at small KA; however, with increasing KA, β drops to values expected for the LW growth rate at constant aerodynamic roughness.

Note that C_β in the laboratory conditions at KA = 0 (Fig. 8) is remarkably larger than for developed seas (Fig. 5). As interpreted, the airflow separation from steep breaking wind-generated SWs in laboratory conditions first provides twice as large of a contribution to the form drag as compared with developed sea conditions (40% vs 20%). Second, for such developed seas, the spectral gap between SW breaking and modulating LWs is much larger. Therefore, because of the relaxation parameter [see (19)], the amplitude of the SW MTF for developed seas is smaller than under laboratory conditions. Both factors can thus explain the larger growth of the LW in such conditions.

5. Conclusions

In this paper, we specifically explored the potential role of short-scale breaking modulations to amplify the growth rate of modulating longer waves. Using the KCM2014 framework, the airflow separations from modulated breaking waves (the form drag modulation) result in strong modulation of the turbulent stress in the inner region of the modulating longer waves. This effect amplifies the growth rate of modulating waves via (i) direct work of the form drag against the wave orbital velocity (maser mechanism of wave generation; Longuet-Higgins 1969) and (ii) amplification of the slope-correlated surface pressure. The latter impact of wave breaking modulations is more efficient (by a factor about 2.5) than their impact via the maser mechanism. As derived, such a mechanism is very efficient and can apparently reconcile the nonseparate sheltering generation mechanism (Belcher and Hunt 1993) with observations, amplifying the wind-wave growth rate by a factor of 2–3.

The suggested model is verified against measurements of the wave growth rate in well-controlled laboratory conditions (Makin et al. 2007; Peirson and Garcia 2008; Grare et al. 2013). An observed decrease of the wave growth rate with the increase of the wave steepness is considered experimental evidence of the validity of the suggested mechanism. For small LW steepness, the modulation of the breaking SWs significantly amplifies the growth of modulating LWs. For large LW steepness, SWs are suppressed and the LW surface becomes aerodynamically ''smooth,'' resulting in a deceleration of the LW growth.

Variations of breaking SWs and the associated aerodynamic roughness along the LW thus certainly crucially affect the wind-induced growth rate of the modulating LW. Yet, it must be pointed out that there is a serious lack of experimental data on the wave breaking modulations. More precise empirical and theoretical knowledge of the spectral distribution of breaking waves and their contribution to the surface drag, as well as breaking SW modulation by longer surface waves, are thus necessary to further advance a more consistent understanding of the wind-wave growth.

Acknowledgments. Funding by the Russian Federation Government Grant 11.G34.31.0078 and Russian Science Foundation Grant 15-17-20020 for this study, and ongoing support under RFBR Grant 14-05-91760/14, the Ministry of Science and Education Project 5.2483.2014/K, and the ESA STSE OceanFlux GHG Evolution Project are gratefully acknowledged. We thank the anonymous referees, who made very helpful comments and suggestions.

REFERENCES

Banner, M. L., I. S. F. Jones, and J. C. Trinder, 1989: Wavenumber spectra of short gravity waves. *J. Fluid Mech.*, **198**, 321–344, doi:10.1017/S0022112089000157.

Belcher, S. E., and J. C. R. Hunt, 1993: Turbulent shear flow over slowly moving waves. *J. Fluid Mech.*, **251**, 109–148, doi:10.1017/S0022112093003350.

——, and ——, 1998: Turbulent flow over hills and waves. *Annu. Rev. Fluid Mech.*, **30**, 507–538, doi:10.1146/annurev.fluid.30.1.507.

Chen, G., and S. E. Belcher, 2000: Effects of long waves on wind-generated waves. *J. Phys. Oceanogr.*, **30**, 2246–2256, doi:10.1175/1520-0485(2000)030<2246:EOLWOW>2.0.CO;2.

Donelan, M. A., and W. J. Pierson, 1987: Radar scattering and equilibrium ranges in wind-generated waves with application to scatterometry. *J. Geophys. Res.*, **92**, 4971–5029, doi:10.1029/JC092iC05p04971.

Dulov, V., V. Kudryavtsev, and A. Bol'shakov, 2002: A field study of whitecap coverage and its modulations by energy containing waves. *Gas Transfer at Water Surfaces, Geophys. Monogr.*, Vol. 127, Amer. Geophys. Union, 187–192.

Elfouhaily, T., B. Chapron, K. Katsaros, and D. Vandermark, 1997: A unified directional spectrum for long and short wind-driven waves. *J. Geophys. Res.*, **102**, 15 781–15 796, doi:10.1029/97JC00467.

Garrett, C., and J. Smith, 1976: On the interaction between long and short surface waves. *J. Phys. Oceanogr.*, **6**, 925–930, doi:10.1175/1520-0485(1976)006<0925:OTIBLA>2.0.CO;2.

Gent, P. R., and P. A. Taylor, 1976: A numerical model of the air flow above water waves. *J. Fluid Mech.*, **77**, 105–128, doi:10.1017/S0022112076001158.

Grare, L., W. L. Peirson, H. Branger, J. W. Walker, J.-P. Giovanangeli, and V. Makin, 2013: Growth and dissipation of wind-forced, deep water waves. *J. Fluid Mech.*, **722**, 5–50, doi:10.1017/jfm.2013.88.

Hunt, J., S. Belcher, D. Stretch, S. Sajjadi, and J. Clegg, 2011: Turbulence and wave dynamics across gas–liquid interfaces. *Gas Transfer at Water Surfaces*, S. Komori, W. McGillis, and R. Kurose, Eds., Kyoto University Press, 1–12.

Janssen, P., 2004: *The Interaction of Ocean Waves and Wind.* Cambridge University Press, 300 pp.

Kudryavtsev, V. N., and V. K. Makin, 2002: Coupled dynamics of short wind waves and the air flow over long surface waves. *J. Geophys. Res.*, **107**, 3209, doi:10.1029/2001JC001251.

——, B. Chapron, and V. Makin, 2014: Impact of wind waves on the air-sea fluxes: A coupled model. *J. Geophys. Res. Oceans*, **119**, 1217–1236, doi:10.1002/2013JC009412.

Longuet-Higgins, M. S., 1969: A nonlinear mechanism for the generation of sea waves. *Proc. Roy. Soc. London*, **311A**, 371–389, doi:10.1098/rspa.1969.0123.

Maat, N., and V. K. Makin, 1992: Numerical simulation of air flow over breaking waves. *Bound.-Layer Meteor.*, **60**, 77–93, doi:10.1007/BF00122062.

Makin, V. K., and V. Kudryavtsev, 2002: Impact of dominant waves on sea drag. *Bound.-Layer Meteor.*, **103**, 83–99, doi:10.1023/A:1014591222717.

——, H. Branger, W. L. Peirson, and J.-P. Giovanageli, 2007: Stress above wind-plus-paddle waves: Modelling of laboratory experiment. *J. Phys. Oceanogr.*, **37**, 2824–2837, doi:10.1175/2007JPO3550.1.

Mastenbroek, C., 1996: Wind wave interaction. Ph.D. thesis, Delft Technical University, 119 pp.

Miles, J. W., 1957: On the generation of surface waves by shear flows. *J. Fluid Mech.*, **3**, 185–204, doi:10.1017/S0022112057000567.

Peirson, W. L., and A. W. Garcia, 2008: On the wind-induced growth of slow water waves of finite steepness. *J. Fluid Mech.*, **608**, 243–274, doi:10.1017/S002211200800205X.

——, H. Branger, J. P. Giovannangeli, and M. L. Banner, 2004: The response of wind drag to underlying swell slope. University of New South Wales Water Research Laboratory Research Rep. 223, 51 pp.

Phillips, O. M., 1985: Spectral and statistical properties of the equilibrium range in the wind-generated gravity waves. *J. Fluid Mech.*, **156**, 505–531, doi:10.1017/S0022112085002221.

Plant, W. J., 1982: A relation between wind stress and wave slope. *J. Geophys. Res.*, **87**, 1961–1967, doi:10.1029/JC087iC03p01961.

Smith, J. A., 1986: Short surface waves with growth and dissipation. *J. Geophys. Res.*, **91**, 2616–2632, doi:10.1029/JC091iC02p02616.

Sullivan, P. P., J. C. McWilliams, and C. H. Moeng, 2000: Simulation of turbulent flow over idealized water waves. *J. Fluid Mech.*, **404**, 47–85, doi:10.1017/S0022112099006965.

Yang, D., C. Meneveau, and L. Shen, 2013: Dynamic modelling of sea-surface roughness for large-eddy simulation of wind over ocean wavefield. *J. Fluid Mech.*, **726**, 62–99, doi:10.1017/jfm.2013.215.

Yurovskaya, M. V., V. A. Dulov, B. Chapron, and V. N. Kudryavtsev, 2013: Directional short wind wave spectra derived from the sea surface photography. *J. Geophys. Res. Oceans*, **118**, 4380–4394, doi:10.1002/jgrc.20296.